Journal Pre-proofs

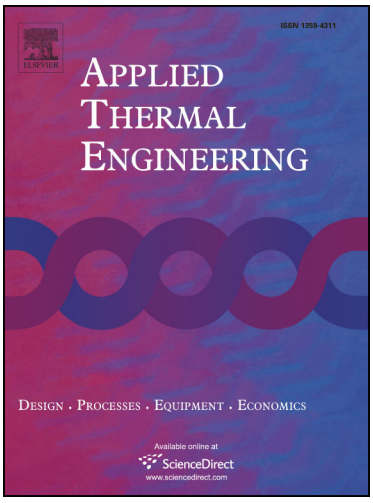

Measurement of thermal conductivity of millimeter-sized wires using the fin effect

Swapnil S. Salvi, Ankur Jain

PII: S1359-4311(20)32964-1
DOI: https://doi.org/10.1016/j.applthermaleng.2020.115482
Reference: ATE 115482

To appear in: *Applied Thermal Engineering*

Received Date: 14 November 2019
Revised Date: 15 April 2020
Accepted Date: 12 May 2020

Please cite this article as: S.S. Salvi, A. Jain, Measurement of thermal conductivity of millimeter-sized wires using the fin effect, *Applied Thermal Engineering* (2020), doi: https://doi.org/10.1016/j.applthermaleng.2020.115482

Measurement of thermal conductivity of millimeter-sized wires using the fin effect

Swapnil S. Salvi, Ankur Jain*

Mechanical and Aerospace Engineering Department
University of Texas at Arlington, Arlington, TX, USA.

* – Corresponding Author: email: jaina@uta.edu;
500 W First St, Rm 211, Arlington, TX, USA 76019
Ph: +1 (817) 272-9338; Fax: +1 (817) 272 2952

Abstract

Measurement of thermal conductivity of thin wires is critical for multiple engineering applications that involve heat transfer in thin wires. While well-established experimental methods are available for thermal conductivity measurements on large as well as microscale samples, these methods do not work well for thin wires of around a few mm diameter. This paper presents a comparative method for measuring thermal conductivity of a thin wire. The method is based on infrared thermography of the wire of interest suspended from a high temperature base. Through comparison of thermal response of the wire with that of a standard wire of known properties, thermal conductivity is measured for a number of wires in a broad range of thermal conductivity. Measurements are reported for both low thermal conductivity polymer wires and high thermal conductivity metal wires. Results are found to be in good agreement with expected values of thermal conductivity. The effect of wire diameter and base temperature on the accuracy of measurements is investigated. The method is used for measurement of thermal conductivity of solder wires. Results presented in this work contribute towards addressing an important thermal

metrology need, and may help improve thermal design of a broad range of engineering applications that utilize thin wires.

Keywords: Thermal Conductivity Measurement; Thin Wires; Infrared Thermography; Fin Effect.

Nomenclature

A_c	Cross-sectional area, m^2
D	Diameter, m
h	Convective heat transfer coefficient, W/m^2K
k	Thermal conductivity, W/mK
L	Sample thickness, m
l	Length, m
m	Slope of semilog plot of temperature distribution, m^{-1}
P	Perimeter, m
T	Temperature, K
t	Time, s
x	Spatial co-ordinates, m
α	Thermal diffusivity, m^2/s
θ	Temperature rise, K

Subscripts:

a	Ambient
b	Base
max	Maximum
S	Standard wire
T	Test wire

1. Introduction

Measuring and understanding the nature of thermal conductivity is important for thermal characterization of materials and for maximizing performance and thermal safety of a variety of engineering devices and systems. As defined by Fourier law, thermal conductivity is a key thermophysical property that relates heat flux with temperature rise. While in general, thermal conductivity is anisotropic and a function of temperature, it is often treated, within engineering approximation to be isotropic and independent of temperature.

A number of experimental techniques exist for measurement of thermal conductivity. In general, these methods rely on measurement of the thermal response of the sample of interest to an imposed heat flux or temperature gradient [1–3]. The experimentally measured thermal response is usually compared with an analytical heat transfer model to determine thermal conductivity. For example, in a commonly used measurement method [2], the material of interest is sandwiched between two plates maintained at two different temperatures, and the measured heat flux is compared with the Fourier law to determine thermal conductivity. Measurements are often carried out on two samples of different thicknesses to account for sample-to-instrument thermal contact resistance [4]. A sample of well-known thermal conductivity is also often inserted in series in order to accurately measure heat flux. A guard heater [5] is often used to minimize stray heat losses. Transient measurements [1,6] are also often used to measure thermal conductivity. For example, the transient plane source method [3] utilizes a thin film metal heater/sensor sandwiched between two large, identical samples. The measured temperature as a function of time is compared with an analytical model for heat transfer into infinite media to determine thermal conductivity. In the laser flash method [7], an energy pulse is deposited on one face of a sample and temperature rise on the other face is measured using an infrared sensor. Comparison with a well-known

analytical model results in determination of thermal diffusivity. Comparison of thermal response of the sample with that of a material of well-known properties is used to determine heat capacity, so that thermal conductivity can then be calculated. Each of these methods offers certain advantages and disadvantages. For example, the laser flash method is non-contact and does not involve thermal contact resistance [8]. However, this method requires extensive sample preparation. On the other hand, the transient plane source requires samples of a certain minimum size depending on the expected thermal diffusivity and measurement capability [9,10].

In addition to the macroscale thermal property measurement techniques summarized above, a number of techniques developed specifically for microscale material samples are also available. In general, most of these methods may be classified into electrical-based [11,12] and optical-based methods [13–15]. In the first category, Joule heating in the form of direct [12,16] or alternating current [11,17] is imposed and the ensuing thermal response is used to determine thermal conductivity. The three-omega method [18] is an example, which has been extensively used for a variety of applications [19,20,21]. In optical methods, heating is provided using an optical signal, and temperature is also usually measured optically in a pump-and-probe configuration. Thermoreflectance based methods [22] are another good example of optical-based methods. Such methods have been extensively used for characterization of thermal properties of micro- and nano-scale materials [23], as well as for more macroscale materials [24,25].

Unfortunately, most measurement techniques outlined above are not appropriate for thin wires. For example, while imposing and measuring a steady-state heat flux through a flat sample of large cross-section is easily implemented in measurement methods, doing so on a wire is challenging due to difficulties in precisely measuring heat flux through the thin wire, as well as

heat loss from the wire perimeter. Several engineering applications such as electrical wires, filaments for additive manufacturing, solder wires, welding electrodes, etc. involve heat transfer in wires, and therefore, understanding thermal conductivity of wires for these applications is critical. For example, in polymer-based additive manufacturing, understanding thermal conduction in the filament is critical for ensuring good filament-to-filament adhesion [26,27]. As another example, the reliability and life time of a non-consumable welding electrode depends critically on its heat dissipation capabilities in the controlled atmosphere [28,29]. Finally, heat transfer in solder wires is also important for ensuring good process quality [30,31], and therefore, understanding thermal conductivity of the solder wires is important. While the thermal conductivity of molten solder material has been reported [32], similar data are not available for solid solder wire.

Despite the importance of understanding and characterizing heat transfer in applications discussed above, there is a lack of systematic measurement methods for thin wires. A recent paper presented a fin-based method to compare thermal conduction in two strands of hair and correlate with moisture content and hair type [33]. However, this work did not report absolute values of the thermal conductivities of the hair being investigated.

This paper presents an experimental technique to measure the thermal conductivity of thin wires using infrared thermography based measurement of temperature distribution along the wires when suspended from a high temperature block. The method is based on comparison of thermal response of the test wire with that of a standard wire of known thermal conductivity in the same surrounding environment. Wires of materials of a broad range of thermal conductivity are characterized. Good accuracy is reported for both low and high thermal conductivity wires. As an application of this measurement technique, thermal conductivity values of different solders are

measured and reported. The fundamental theory behind this method utilizes the fin effect, which is quite standard, however, measurement of thermal conductivity of wires based on this approach has not been reported in the past.

Theoretical modeling of the measurement method is discussed in section 2. Experimental setup and experimental procedure is presented in Section 3. Results are presented and discussed in section 4.

2. Theoretical Treatment

Consider a long cylindrical wire of length l and diameter D, for which, measurement of axial thermal conductivity k is of interest. k is assumed to be constant and isotropic. As shown in Figure 1(b), consider the wire to be attached at one end to a large body maintained at a constant temperature T_b. The wire loses heat from its periphery to the ambient temperature T_a due to convection. The wire is assumed to be long enough, so that the infinite fin assumption is appropriate for analytical modeling. The validity of this assumption for the wires used in this work is discussed in Section 4.5. Aspect ratio of the wire is assumed to be very large, so that thermal conduction in the wire is one-dimensional. Further, the radial Biot number is calculated to be 0.04 or less for the experimental conditions, due to which, thermal gradient in the radial direction is expected to be negligible. Temperature rise during the experiment is assumed to be small enough, such that radiative heat transfer can be modeled using a linearized radiative heat transfer coefficient. . Under these conditions, steady state temperature distribution in the wire is governed by the well-known fin equation [34]

$$\frac{d^2\theta}{dx^2} - \frac{hP}{kA_C}\theta = 0 \tag{1}$$

Where, $\theta = T(x) - T_a$ is the temperature rise above ambient. Further, $P = \pi D$ and $A_C = \frac{\pi D^2}{4}$ are the perimeter and cross-section area, respectively. *h* is the effective heat transfer coefficient that accounts for both convection and radiation and is assumed to be independent of temperature. Boundary conditions associated with equation (1) are

$$\theta(x = 0) = \theta_b \tag{2}$$

$$\theta \to 0 \ \ as \ \ x \to \infty \tag{3}$$

Temperature distribution in the fin can be easily derived to be [34]

$$\frac{\theta}{\theta_b} = e^{-mx} \tag{4}$$

where $m^2 = \frac{hP}{kA_c}$.

Equation (4) shows that the parameter *m* can be determined from the slope of the plot of $\log(\theta/\theta_b)$ versus *x*. Further, provided the wire geometry and convective heat transfer coefficient *h* are known, the unknown thermal conductivity of the wire can be determined. However, while the wire geometry is usually known in advance, convective heat transfer around the wire is, in general, very difficult to measure, and therefore, a definitive value of *h* is not known.

In order to determine thermal conductivity without explicitly knowing the convective heat transfer coefficient, a comparative analysis is considered, wherein two wires – a test wire T of unknown thermal conductivity k_T and standard wire S of known thermal conductivity k_S – are considered. Both wires are subjected to the same ambient conditions, such as shown in Figures 1(a) and 1(b), so that the ratio of the slopes of $\log(\theta/\theta_b)$ versus x plots for the two wires is given by

$$\frac{m_S}{m_T} = \sqrt{\frac{k_T D_T}{k_S D_S}} \tag{5}$$

Equation (5) assumes the same convective heat transfer coefficient for both wires, which is reasonable if the two wires are of similar diameter and are measured simultaneously in the same ambient conditions. Equation (5) can be simplified to

$$k_T = k_S \frac{m_S^2 D_S}{m_T^2 D_T} \tag{6}$$

Equation (6) shows that the unknown thermal conductivity of the test wire, k_T, can be determined from the known thermal conductivity of the standard wire, k_S, based on the ratio of wire diameters, as well as the ratios of the m^2 values determined from experimental measurement of temperature distributions along the wires. Such a measurement will require a method such as infrared thermography to determine the entire temperature distribution along the wire in a non-contact manner. Note that while equation (6) indicates that the test and standard wires may be chosen to have different diameters, significantly different diameters may result in different

convective heat transfer coefficient, since convective heat transfer from a heated wire in general depends on the wire diameter [34-36] in both forced and natural convection conditions.

Even though the theory outlined above is based on the well-known fin effect [34], the authors are unaware of the use of these results for measurement of thermal conductivity of wires, as described above.

The next section discusses experimental design and setup for thermal conductivity measurement.

3. Experiments

Based on the theoretical method described in Section 2, experiments are carried out to measure the thermal conductivity of thin wires in a broad range of thermal conductivity values.

3.1. Experimental setup

As shown in Figure 1(a), the test wire with unknown thermal conductivity and a standard wire with known thermal conductivity are both suspended from a 25 mm by 25 mm by 25 mm Aluminum block using a metallic wire holding fixture that is designed to position the wires horizontally. The two wires are mounted close to each other, so that both experience the same ambient conditions, but not too close so that there is no thermal cross-talk. Through trial experiments, it is found that a wire-to-wire gap of 3.0 mm results in no thermal interactions between the two wires, whereas lower gaps are found to result in undesirable heat transfer between wires. Therefore, all experiments in this paper are carried out with a wire-to-wire gap of 3.0 mm. The theoretical model in section 2 assumes that radiation can be accounted for with a linear

radiative heat transfer coefficient, and that temperature-dependence of the convective heat transfer coefficient is negligible. The temperature rise in experiments is limited to 20 °C in order to ensure that the validity of these assumptions.

The positioning of wires relative to the infrared camera lens can be altered using a dial operated sliding table arrangement. The Aluminum block is placed on an Instec HCS662V thermal stage that can be maintained at a constant temperature. Thermal interface material is applied between the Aluminum block and Instec stage, as well as between the block and wires to minimize interfacial temperature drop. Temperature distribution along the wires is measured using an FLIR A6703sc InSb infrared camera with a spatial resolution of around 15μm and Noise Equivalent Temperature Difference of around 20 mK. Both wires are thermally imaged simultaneously. In each case, the wire length is chosen in order to satisfy the long wire assumption of the theoretical model. Depending on the wire length, this may result in measurement of only a portion of the long wire at a time instead of the entire wire. Additional length of the wire can be measured by moving the positioning stage that results in linear shift of the wire with respect to the infrared camera. Both wires are coated with a thin graphite spray in order to ensure uniform surface emissivity. Since the graphite spray is only a very thin film, it is not expected to significantly change thermal properties of the wire. Similar to past experiments [37,38], calibration of the infrared camera is carried out in advance. Infrared emission from a surface coated with the graphite spray is measured at a number of known temperatures, and the emissivity is chosen to be the value that results in closest agreement between the known temperatures and those determined from the measured infrared emission.

Figure 1(a) presents a picture of the experimental setup. Figure 1(b) depicts a schematic of the experimental setup, including dimensions and coordinate systems for the theoretical model.

3.2. Experimental procedure

Several experiments are carried out on high *k* metal and low *k* polymer wires using suitable standard wires of known thermal conductivity. In each case, the wires are chosen to be around 60 mm and 300 mm long for polymers and metals, respectively. Infrared thermography of the entire wire is carried out to ensure that the infinite fin assumption is valid. This is discussed in more detail in Section 4.5. Since temperature distribution in the wire decays exponentially, temperature rise in the wire closer to the tip can be small and noisy, which can distort the thermal conductivity measurement. Accordingly, temperature measurement close to the tip is not considered for determining thermal conductivity. The length of the wire to be considered for thermal conductivity measurements is determined by plotting $\log(\theta/\theta_b)$ as a function of x, and determining the length beyond which the plot is not linear due to low and noisy temperature measurement.

In each experiment, the standard wire is chosen to be such that the test and standard thermal conductivities are in the same order of magnitude. This ensures that the slopes of temperature distributions are close to each other and eliminates error inherent in measuring relatively large or small slopes.

In each experiment, the Instec heating stage temperature is set to a specific value and allowed to reach steady state. The set temperature is chosen to be 35 ^{o}C and 45 ^{o}C for polymer and metal wires, respectively. The higher temperature for metallic wires is needed for reasonable signal-to-noise ratio, given the relatively high thermal conductivity of metals. Once thermal steady

state is reached, temperature distribution along each wire is measured using the infrared camera. Both wires are designed to be long enough so that temperature at the tip of the wires is close to ambient temperature. Forced air flow from an external fan is utilized in some experiments, particularly for metal wires, in which case the increased convective heat transfer coefficient due to forced air flow helps achieve the long fin assumption.

3.3. Reference thermal conductivity measurements

Two independent thermal conductivity measurement techniques are used for determining thermal conductivity of standard samples and validation of thermal conductivity measured using the proposed method. The laser flash method involves deposition of a pulse of energy on one face of a thin cylindrical sample while temperature rise on the other face is measured using an infrared detector. An analytical model for heat transfer in the sample [7] shows that temperature rise on the back side of the sample is given by

$$T(t) = T_{max} \cdot \left[1 + 2\sum_{n=1}^{\infty}(-1)^n \exp\left(-\frac{n^2\pi^2\alpha t}{L^2}\right)\right] \tag{7}$$

Where L and α are the sample thickness and thermal diffusivity, respectively. Comparison of experimental data with equation (7) results in determination of thermal diffusivity of the sample. Corrections to account for finite width of the heating pulse are taken into account. Further, comparative measurement of the peak temperature rise between the sample and a standard material is used to determine heat capacity. These measurements together help determine thermal

conductivity of the sample. These measurements are carried out on a Netzsch LFA467 instrument. Since this method requires samples of relatively large diameter, the measurements are carried out on samples made of the same material as the wires of interest. Both wires are purchased from the same manufacturer. This ensures that thermal conductivity of the sample being tested is the same as that of the wire of interest.

A one-dimensional, steady state heat flux method is also used in some cases to independently determine thermal conductivity of the wire materials being investigated in this work. This method, implemented in a TA Instruments Fox50 instrument, sandwiches a thin sample of the material of interest between two plates maintained at different temperatures. Measurement of the resulting heat flux through the material at steady state helps determine total thermal resistance. The effect of thermal contact resistances between the material and hot/cold plates is accounted for by two independent measurements of samples of different thicknesses. Similar to the laser flash method, these measurements are carried out on larger samples made of the material of interest purchased from the same manufacturer.

4. Results and discussion

4.1. Temperature data and comparative determination of k_T

Figure 2(a) presents a raw thermal image at steady state showing simultaneous measurement on two wires – carbon steel (high strength 1045) and nickel alloy steel (thermally stable Invar 36). The wires are arranged parallel to each other with around 3.0 mm gap, and the wire base temperature is maintained at 45 °C. A clear temperature gradient down the wires can be observed for both materials. Temperature gradient normal to the wires is very small, indicating

negligible wire-to-wire heat transfer. Figure 2(b) plots steady state temperature distribution along both wires, showing distinct, non-linear temperature gradient in each case, as expected from fin theory.

Further, Figure 3 plots temperature distribution on a semilog scale at a number of times prior to steady state for a 3.16 mm diameter stainless steel wire. These data show rapid changes in temperature distribution at early times as thermal diffusion from the base into the wire occurs. As time passes, a robust steady state distribution is established, with no significant temperature change beyond around 60 s. The steady-state temperature distribution is found to be linear on the semilog plot, as expected from equation (4). The slope of this curve may be used in accordance with equations (5) and (6) to determine unknown thermal conductivity of a test wire based on known thermal conductivity of a standard wire subjected to the same conditions.

Note that linearity of the semilog plot shown in Figure 3 indicates the validity of the assumption that the heat transfer coefficient around the wire is independent of temperature. If there was significant temperature-dependence, equation (4) would not have been the correct temperature solution, and experimental data would not have resulted in a linear semilog plot of the temperature distribution. For further investigation of this, the wire temperature has been determined based on finite-element simulation as well as numerical solution of the governing energy equation for two different cases – temperature-dependent convective heat transfer coefficient and constant convective heat transfer coefficient. Temperature distributions predicted for both cases are found to be very close to each other.

Comparative experiments to determine thermal conductivity of a wire are summarized in Figures 4 and 5 for low thermal conductivity polymer wires and high thermal conductivity metal

wires, respectively. Figure 4 plots $\log(\theta/\theta_b)$ vs x for two polymer wires – polypropylene and acetal – of around 3.0 mm diameters with base temperature of 35 °C. Plots for both wires shown in Figure 4 are linear, with R^2 value of greater than 0.97 in both cases. The slopes of both plots result in m = 94.76 m^{-1} and 79.31 m^{-1}, respectively. Thermal conductivity of polypropylene, separately measured to be 0.20±0.01 W/mK using a one-dimensional heat flux method described in Section 3, is treated to be a known, standard value. Based on equation (6), thermal conductivity of acetal is then determined to be 0.27±0.01 W/mK, which is within 3.6% of the independently measured value of 0.28±0.02 W/mK using the one-dimensional heat flux method. This demonstrates the capability of the measurement method to determine unknown thermal conductivity of a polymer wire based on known thermal conductivity of another wire.

In order to improve measurement accuracy, thermal conductivities of the standard and test wires must be of the same order of magnitude. Therefore, for thermal measurements on metal wires, the standard wire must have similarly high thermal conductivity. This is investigated in Figure 5 that presents experimental data for Aluminum (6061) and Copper (110) wires of around 3.0 mm diameter with a base temperature of 45 ^{o}C. Unlike polymer wires, experiments for metal wires are carried out in the presence of forced convective cooling due to air flow at around 7.8 m/s from a fan. This is needed for metal wires in order to ensure a reasonable rate of decay of temperature along the wire and higher signal-to-noise ratio. Similar to polymer wires, linear temperature decay on the semilog plot is observed for metal wires, which is consistent with equation (4). The R^2 values are greater than 0.99 for both copper and aluminum wires. In this case, aluminum is treated as the standard wire. Thermal conductivity of a 25.4 mm diameter and 2.67 mm thickness sample machined from the same material as the wire is determined in advance using the laser flash method to be 182.7±9.1 W/mK. Based on this, thermal conductivity of the copper

wire is determined using equation (6) to be 401.5±26.5 W/mK. This compares well with an independent laser flash measurement of 403.2±20.2 W/mK as well as the manufacturer-specified value of 390.9 W/mK.

Figures 4 and 5 together demonstrate the capability of the method described in Sections 2 and 3 to accurately measure thermal conductivity over a wide range of values, covering both low thermal conductivity materials such as polymers and high thermal conductivity materials such as metals.

A series of additional measurements are also carried out for both polymers and metals, using different materials as standard. These data are summarized in Tables 1 and 2 for metal and polymer materials, respectively. Very good agreement with independently measured or manufacturer-provided values for thermal conductivity are observed in each case, thereby demonstrating the versatility of the measurement method. Note that Aluminum is used as standard for relatively high thermal conductivity metals, while Carbon Steel is used as standard for relatively low thermal conductivity metals. Thermal conductivity of both Aluminum and Carbon Steel are measured independently using laser flash method.

4.2. Measurements on wires of different diameters

As shown in equation (4), wire size plays a key role in determining the value of m, and hence in the measurement of thermal conductivity. Figure 6 plots $\log(\theta/\theta_b)$ vs x for two wires of the same material – Brass (360) – but different diameters. As expected, the rate of temperature drop is greater for the thinner wire due to larger value of m for smaller diameter wires. Equation (5) shows that for wires of different diameters but the same material and ambient conditions, the non-dimensional product $D \times m^2$ must be constant. This product is found to be 6.13 and 5.95 for

the 3.18 mm and 4.74 mm wires, respectively. These values are within 2.9% of each other, indicating that the nature of heat transfer during these experiments is consistent with the theoretical model presented in Section 2. Note that the convective heat transfer coefficient h for two wires of different diameters may be somewhat different even when subjected to the same ambient conditions. This is because convective heat transfer from a heated wire is, in general, a function of the wire diameter. In the case of forced convection, as the wire diameter increases, convective heat transfer coefficient decreases [36], and therefore, m reduces. Similarly, natural convection heat transfer coefficient also depends on the wire diameter. Based on well-known correlations for convective heat transfer from cylinders [34–36], it is found that for natural convection, this is not a significant effect around 2-6 mm diameter wires in air. On the other hand, for forced convection, this is not a significant effect for wires greater than around 2 mm diameter in air. Therefore, within these ranges, choosing different diameters for the test and standard samples may be acceptable.

Figure 7 presents data for an even more general case where the two wires have different diameters and are of different materials. Specifically, carbon steel and stainless steel wires of diameters 3.16 mm and 4.77 mm respectively are used, treating carbon steel as the standard wire with a known thermal conductivity of 45.8±2.3 W/mK based on aluminum wire as reference. As shown in Figure 7, linear semilog plots are obtained in this case, similar to prior experiments. Based on the m values determined from the temperature measurement and taking into account the unequal diameters of the wires, thermal conductivity of the stainless steel is found to be 14.1±0.9 W/mK, which is within 2.5% of the manufacturer-provided thermal conductivity of 14.4 W/mK.

4.3. Impact of experimental conditions on measurement accuracy

Figure 8 examines the effect of external air flow on the measurements. Measured temperature distributions for the same 3.15 mm diameter copper wire subjected to three different convective cooling conditions are presented. These include natural convection and forced convection at two different fan speeds. As expected, there is greater rate of temperature reduction with increased air flow. In each case, the temperature distribution is found to be linear on the semilog plot, consistent with equation (4). The values of h for these three cases obtained by data fitting and based on the known thermal conductivity of the copper wire are found to be 14, 135 and 209 W/m^{2}K, respectively, which, as expected increase with fan speed. While it is not claimed that the heat transfer coefficient can be measured in this manner, these data demonstrate consistency between experimental measurements and the theoretical model discussed in Section 2.

The effect of base temperature on the measurements is examined next. Theoretically, the base temperature is not expected to influence measurements, since it does not impact the slope m of the $\log(\theta/\theta_b)$ vs x plot. However, a low base temperature results in low overall temperature rise in the wire, leading to greater noise relative to the higher wire temperature rise. In order to examine this effect, temperature distribution for a 3.15 mm diameter copper wire is plotted for three different base temperatures in Figure 9, keeping convective cooling conditions the same. It is observed that greater base temperature results in significant reduction in noise. The higher the base temperature, the greater is the R^2 value of the linear fit, and thus the greater is the accuracy in thermal conductivity measurement. However, the base temperature should not be so large that secondary effects such as radiative heat transfer and natural convective motion due to the hot base become important. This is an important consideration since natural convection close to the base may result in axially varying convective heat transfer coefficient, which is not captured by the

analytical model presented here. Further, for measurements of thermal conductivity as a function of temperature, the temperature range in each measurement must be designed to be as low as possible, while still ensuring reasonable signal-to-noise ratio. Such trade-offs are important to consider for effective design of a thermal conductivity measurement experiment based on the technique discussed in this paper.

4.4. Measurement of thermal conductivity of solder wires

Finally, in order to demonstrate the application of this technique, thermal conductivities of a variety of solder wires are measured. 3.16 mm diameter carbon steel wire is used as the standard wire for each solder wire measurement. As discussed in section 4.1, thermal conductivity of carbon steel is independently measuring using a laser flash method. Table 3 summarizes the measurement results for machine solder, solder for drinking water, torch solder and rosin flux core solders. Note that both torch solder and rosin flux core solders have the same outer diameter and composition of 60% Lead and 40% Tin. However, the rosin flux core solder has an inner core of flux material, with the solder material forming an annular ring. The measured thermal conductivities of 40.6±2.6 W/mK and 31.3±2.0 W/mK are consistent with the material composition, as the presence of low thermal conductivity flux material is expected to result in lower thermal conductivity of the rosin flux core solder wire. The thermal distinction between the two wires is also clear from the comparative thermal measurement shown in Figure 10.

4.5. Validity of infinite fin assumption

A key assumption made in the theoretical model presented in Section 2 is that the wire is infinitely long. This assumption facilitates derivation of the temperature distribution, equation (4), without needing to know the thermal state of the fin tip. In order to verify the appropriateness of

the infinite fin assumption for wires investigated in this work, temperature distribution for the entire length of two representative wires – one polymer and the other metal – are plotted in Figure 11. These data clearly show that for both wires, temperature reduces to the ambient temperature within the wire length, thus showing that the infinite fin assumption is applicable. Note that even though the choice of the overall wire length is dictated by the infinite fin assumption, measurement of thermal conductivity is based on temperature rise in only a shorter section of the wire, typically the first three quarter-lengths of the wire, where the temperature rise is reasonably large. Beyond this length, temperature rise is found to be small/noisy, and is, therefore, neglected for determining thermal conductivity.

4.6. Uncertainty analysis

Error propagation analysis is carried out in order to estimate the uncertainty in thermal conductivity measurements reported here. Differentiating equation (6) results in

$$\frac{\partial k_T}{k_T} = \frac{\partial k_S}{k_S} + \frac{\partial D_S}{D_S} + \frac{\partial D_T}{D_T} + 2\frac{\partial m_S}{m_S} + 2\frac{\partial m_T}{m_T} \tag{8}$$

The relative error in measurement of the thermal conductivity of standard wire material, based on laser flash technique and one-dimensional steady state heat flux methods described in section 3.3, is estimated to be 5% and 4% respectively, based on manufacturer specifications. Uncertainty in measurement of wire diameter is estimated based on the least count of 0.01 mm of the Vernier caliper used. Finally, uncertainties in the slopes m_S and m_T may occur due to error in infrared temperature measurement. A linear regression analysis of the measured temperature distribution along the wire, accounting for the manufacturer-specified maximum error in infrared temperature measurement, is carried out. This is found to be result in an uncertainty of less than

0.25% for metals and 0.40% for polymers in each slope. Combining all of the uncertainties, the uncertainty in measurement of thermal conductivity of the test wire is estimated to be around 6.1% for the case of acetal based on polypropylene. Similar uncertainties are estimated for other measurements as well, and are listed in Tables 1-3.

Note that once the thermal conductivity of a wire has been measured by comparison against a standard wire, the wire can, in principle, then be used a standard wire to measure thermal conductivity of other wires as well. However, this is not recommended, since this may lead to significant uncertainty propagation. Thermal conductivity of the standard wire must always be determined through an independent measurement. Only when an independently-measured wire is not available at all for use as standard, should a previously-measured wire be considered as a standard, and even then, in doing so, one must recognize the possibility of increased measured uncertainty.

5. Conclusions

This work directly addresses an important thermal metrology need for thermal characterization of thin wires that are used in a variety of engineering applications. The size of such wires often makes them unsuitable for both macroscale and microscale thermal conductivity measurement techniques. Using the well-known fin effect, this work develops a novel technique for determining thermal conductivity of a thin wire through a comparative measurement with a standard wire. Due to the small value of the radial Biot number, this method directly measures the axial thermal conductivity of the wire. Further, note that the method relies on a constant heat transfer coefficient around the wire, which is a reasonable assumption for the small temperature

rise in the present experiments, but may break down due to non-linear radiative heat transfer at larger temperature differences. Results are shown to be in good agreement with independent measurements.

The technique discussed here offers key advantages over traditional techniques such as laser flash and transient plane source methods, which are not applicable for direct measurements on wires. Further, the method is non-invasive and is unaffected by thermal contact resistances, since temperature measurement is carried out using an infrared camera. The method may be applicable for a number of applications where thermal performance of wires is important to understand and optimize.

REFERENCES

[1] Azarfar, S., Movahedirad, S., Sarbanha, A. A., Norouzbeigi, R., and Beigzadeh, B., 2016, "Low Cost and New Design of Transient Hot-Wire Technique for the Thermal Conductivity Measurement of Fluids," Appl. Therm. Eng., **105**, pp. 142–150.

[2] Zhao, D., Qian, X., Gu, X., Jajja, S. A., and Yang, R., 2016, "Measurement Techniques for Thermal Conductivity and Interfacial Thermal Conductance of Bulk and Thin Film Materials," J. Electron. Packag., **138**(4), p. 040802.

[3] Al-Ajlan, S. A., 2006, "Measurements of Thermal Properties of Insulation Materials by Using Transient Plane Source Technique," Appl. Therm. Eng., **26**(17–18), pp. 2184–2191.

[4] Nan, C. W., Birringer, R., Clarke, D. R., and Gleiter, H., 1997, "Effective Thermal Conductivity of Particulate Composites with Interfacial Thermal Resistance," J. Appl. Phys., **81**(10), pp. 6692–6699.

[5] Xamán, J., Lira, L., and Arce, J., 2009, "Analysis of the Temperature Distribution in a Guarded Hot Plate Apparatus for Measuring Thermal Conductivity," Appl. Therm. Eng., **29**(4), pp. 617–623.

[6] Mathis, N., 2000, "Transient Thermal Conductivity Measurements: Comparison of Destructive and Nondestructive Techniques," High Temp. - High Press., **32**(3), pp. 321–327.

[7] Parker, W. J., Jenkins, R. J., Butler, C. P., and Abbott, G. L., 1961, "Flash Method of Determining Thermal Diffusivity, Heat Capacity, and Thermal Conductivity," J. Appl. Phys., **32**(9), pp. 1679–1684.

[8] Min, S., Blumm, J., and Lindemann, A., 2007, "A New Laser Flash System for Measurement of the Thermophysical Properties," Thermochim. Acta, **455**(1–2), pp. 46–49.

[9] Palacios, A., Cong, L., Navarro, M. E., Ding, Y., and Barreneche, C., 2019, "Thermal Conductivity Measurement Techniques for Characterizing Thermal Energy Storage Materials – A Review," Renew. Sustain. Energy Rev., **108**, pp. 32–52.

[10] Ostanek, J., Shah, K., and Jain, A., 2016, "Measurement Sensitivity Analysis of the Transient Hot Source Technique Applied to Flat and Cylindrical Samples," J. Therm. Sci. Eng. Appl., **9**(1), p. 011002.

[11] Wang, H., and Sen, M., 2009, "Analysis of the 3-Omega Method for Thermal Conductivity Measurement," Int. J. Heat Mass Transf., **52**(7–8), pp. 2102–2109.

[12] Zhang, X., Fujiwara, S., and Fujii, M., 2000, "Measurements of Thermal Conductivity and Electrical Conductivity of a Single Carbon Fiber," Int. J. Thermophys., **21**(4), pp. 965–980.

[13] Malen, J. A., Baheti, K., Tong, T., Zhao, Y., Hudgings, J. A., and Majumdar, A., 2011, "Optical Measurement of Thermal Conductivity Using Fiber Aligned Frequency Domain Thermoreflectance," J. Heat Transfer, **133**(8), p. 081601.

[14] Rusconi, R., Rodari, E., and Piazza, R., 2006, "Optical Measurements of the Thermal Properties of Nanofluids," Appl. Phys. Lett., **89**(26).

[15] Popov, Y. A., Pribnow, D. F. C., Sass, J. H., Williams, C. F., and Burkhardt, H., 1999, "Characterization of Rock Thermal Conductivity by High-Resolution Optical Scanning," Geothermics, **28**(2), pp. 253–276.

[16] Vishwakarma, V., and Jain, A., 2014, "Measurement of In-Plane Thermal Conductivity and Heat Capacity of Separator in Li-Ion Cells Using a Transient DC Heating Method," J. Power Sources, **272**, pp. 378–385.

[17] Cahill, D. G., 1990, "Thermal Conductivity Measurement from 30 to 750 K: The 3ω Method," Rev. Sci. Instrum., **61**(2), pp. 802–808.

[18] Oh, D. W., Jain, A., Eaton, J. K., Goodson, K. E., and Lee, J. S., 2008, "Thermal Conductivity Measurement and Sedimentation Detection of Aluminum Oxide Nanofluids by Using the 3ω Method," Int. J. Heat Fluid Flow, **29**(5), pp. 1456–1461.

[19] Qiu, L., Zheng, X. H, Su, G. P., and Tang, D. W., 2013, "Design and Application of a Freestanding Sensor Based on 3ω Technique for Thermal-Conductivity Measurement of Solids, Liquids, and Nanopowders," Int. J. Thermophysics, 34, pp. 2261-2275.

[20] Qiu, L., Tang, D. W., Zheng, X. H, and Su, G. P., 2011, "The freestanding sensor-based 3ω technique for measuring thermal conductivity of solids: Principle and examination," Rev. Sci. Instrum., 82(4), 045106.

[21] L. Qiu, X.H. Zheng, P. Yue, J. Zhu, D.W. Tang, Y.J. Dong, Y.L. Peng, 2015, "Adaptable thermal conductivity characterization of microporous membranes based on freestanding sensor-based 3ω technique," Int. J. Therm. Sci., 89, 186-192.

[22] Wang, X., Shakouri, A., Mavrokefalos, A., Lee, Y., Kong, H., and Shi, L., 2010, "Thermoreflectance Imaging Measurement of In-Plane Thermal Properties of Thin-Film Structures," Annu. IEEE Semicond. Therm. Meas. Manag. Symp., pp. 235–239.

[23] Cahill, D. G., Goodson, K., and Majumdar, A., 2002, "Thermometry and Thermal Transport in Micro/Nanoscale Solid-State Devices and Structures," J. Heat Transfer, **124**(2), p. 223.

[24] Langenberg, E., Ferreiro-Vila, E., Leborán, V., Fumega, A. O., Pardo, V., and Rivadulla, F., 2016, "Analysis of the Temperature Dependence of the Thermal Conductivity of Insulating Single Crystal Oxides," APL Mater., **4**(10), p. 104815.

[25] Zheng, Q., Li, C., Rai, A., Leach, J. H., Broido, D. A., and Cahill, D. G., 2019, "Thermal Conductivity of GaN, 71GaN, and SiC from 150 K to 850 K," Phys. Rev. Mater., **3**(1), p. 014601.

[26] Ravoori, D., Alba, L., Prajapati, H., and Jain, A., 2018, "Investigation of Process-Structure-Property Relationships in Polymer Extrusion Based Additive Manufacturing through in Situ High Speed Imaging and Thermal Conductivity Measurements," Addit. Manuf., **23**, pp. 132–139.

[27] Costa, S. F., Duarte, F. M., and Covas, J. A., 2017, "Estimation of Filament Temperature and Adhesion Development in Fused Deposition Techniques," J. Mater. Process. Technol., **245**, pp. 167–179.

[28] Zhu, P., Lowke, J. J., and Morrow, R., 1992, "A Unified Theory of Free Burning Arcs, Cathode Sheaths and Cathodes," J. Phys. D. Appl. Phys., **25**(8), pp. 1221–1230.

[29] Raoelison, R. N., Fuentes, A., Pouvreau, C., Rogeon, P., Carré, P., and Dechalotte, F., 2014, "Modeling and Numerical Simulation of the Resistance Spot Welding of Zinc Coated Steel Sheets Using Rounded Tip Electrode: Analysis of Required Conditions," Appl. Math. Model., **38**(9–10), pp. 2505–2521.

[30] Wu, D., Huang, C., Ma, Y., Wang, Y., Wang, F., and Guo, C., 2019, "Enhanced Thermal Conductivity of Welding Spots by Coatings Cupric Acetate on Copper Nanoparticle Solders," Mater. Res. Express, **6**(8), p. 085091.

[31] Öztürk, E., Aksöz, S., Keşlioğlu, K., and Maraşlı, N., 2013, "The Measurement of

Thermal Conductivity Variation with Temperature for Sn-20wt.% In Based Lead-Free Ternary Solders," Thermochim. Acta, **554**, pp. 63–70.

[32] Bilek, J., Atkinson, J. K., and Wakeham, W. A., 2006, "Thermal Conductivity of Molten Lead-Free Solders," Int. J. Thermophys., **27**(1), pp. 92–102.

[33] Hahn, J., Marconnet, A., and Reid, T., 2016, "Using Do-It-Yourself Practitioners as Lead Users: A Case Study on the Hair Care Industry," J. Mech. Des., **138**(10), p. 101107.

[34] Incropera, F. P., DeWitt, D. P., Bergman, T. L., and Lavine, A. S., 2007, *Fundamentals of Heat and Mass Transfer*, John Wiley & Sons.

[35] Churchill, S. W., and Chu, H. H. S., 1975, "Correlating Equations for Laminar and Turbulent Free Convection from a Horizontal Cylinder," Int. J. Heat Mass Transf., **18**(9), pp. 1049–1053.

[36] Churchill, S. W., and Bernstein, M., 1977, "A Correlating Equation for Forced Convection From Gases and Liquids to a Circular Cylinder in Crossflow," J. Heat Transfer, **99**(2), p. 300.

[37] Anthony, D., Sarkar, D., and Jain, A., 2016, "Non-Invasive, Transient Determination of the Core Temperature of a Heat-Generating Solid Body," Sci. Rep., **6**(1), p. 35886.

[38] Anthony, D., Wong, D., Wetz, D., and Jain, A., 2017, "Non-Invasive Measurement of Internal Temperature of a Cylindrical Li-Ion Cell during High-Rate Discharge," Int. J. Heat Mass Transf., **111**, pp. 223–231.

List of Figures:

List of Tables:

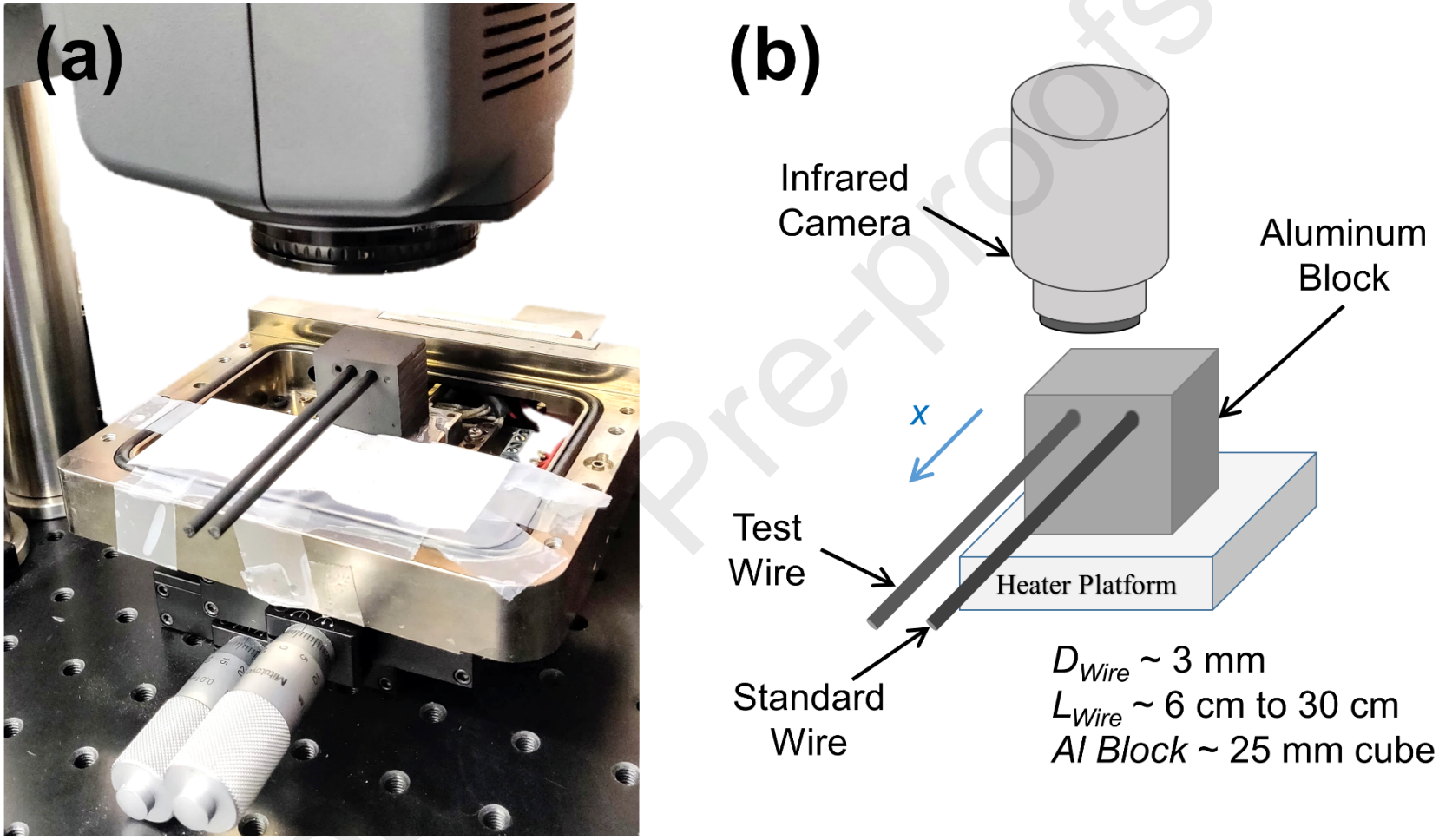

Figure 1: (a) Picture of the experimental setup showing the infrared camera, graphite-coated standard and test wires and a hot Aluminum block, (b) Schematic of the experimental setup.

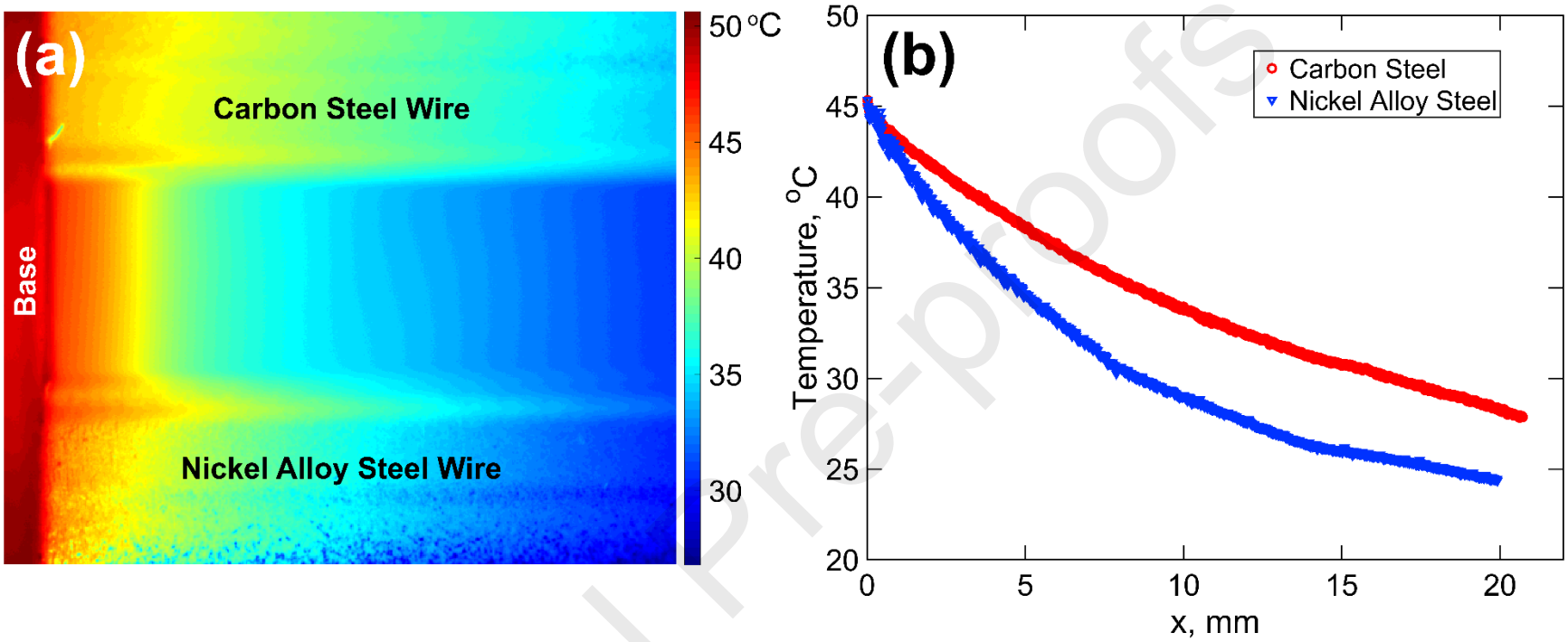

Figure 2 – (a) Raw steady-state infrared thermograph of two wires – carbon steel and nickel alloy steel – of diameters 3.16 mm and 3.18 mm respectively, (b) Steady-state temperature distribution along both wires.

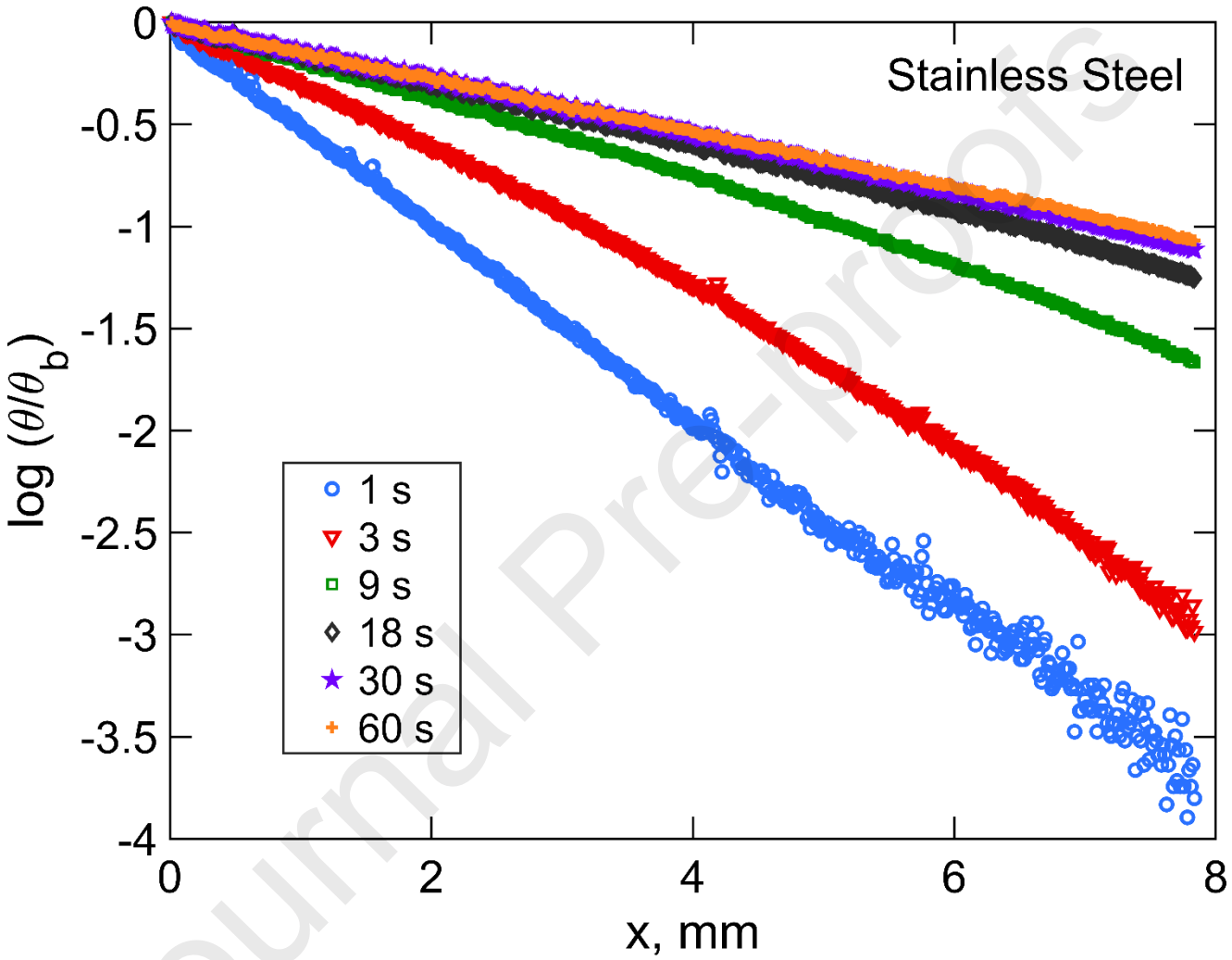

Figure 3: Temperature distribution at multiple times along a stainless steel wire showing establishment of a thermal steady state in approximately 60 s.

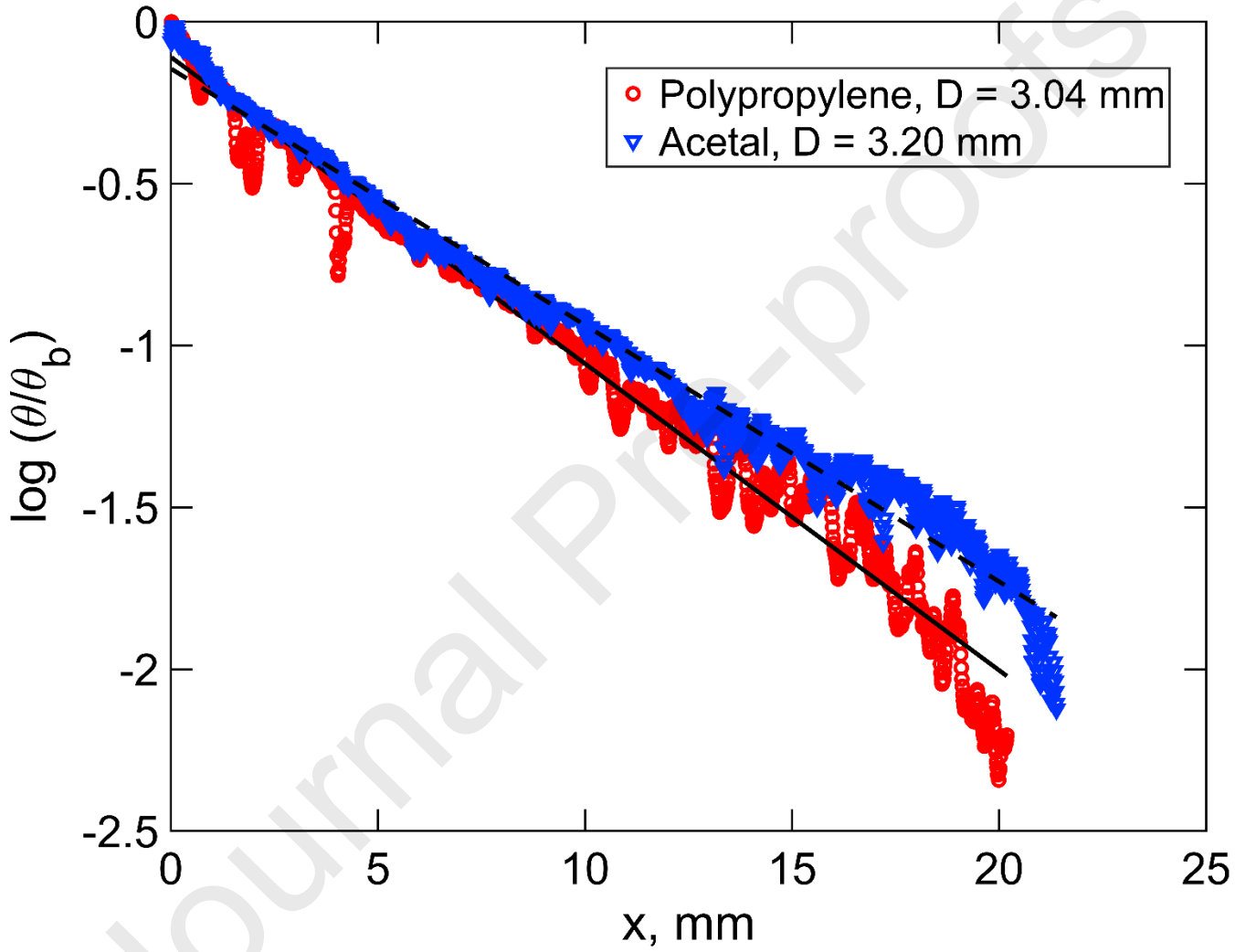

Figure 4: Measured temperature distributions in polypropylene and acetal wires of diameters 3.04 mm and 3.20 mm respectively. Data are plotted on a semilog scale, and linear curve fits are shown.

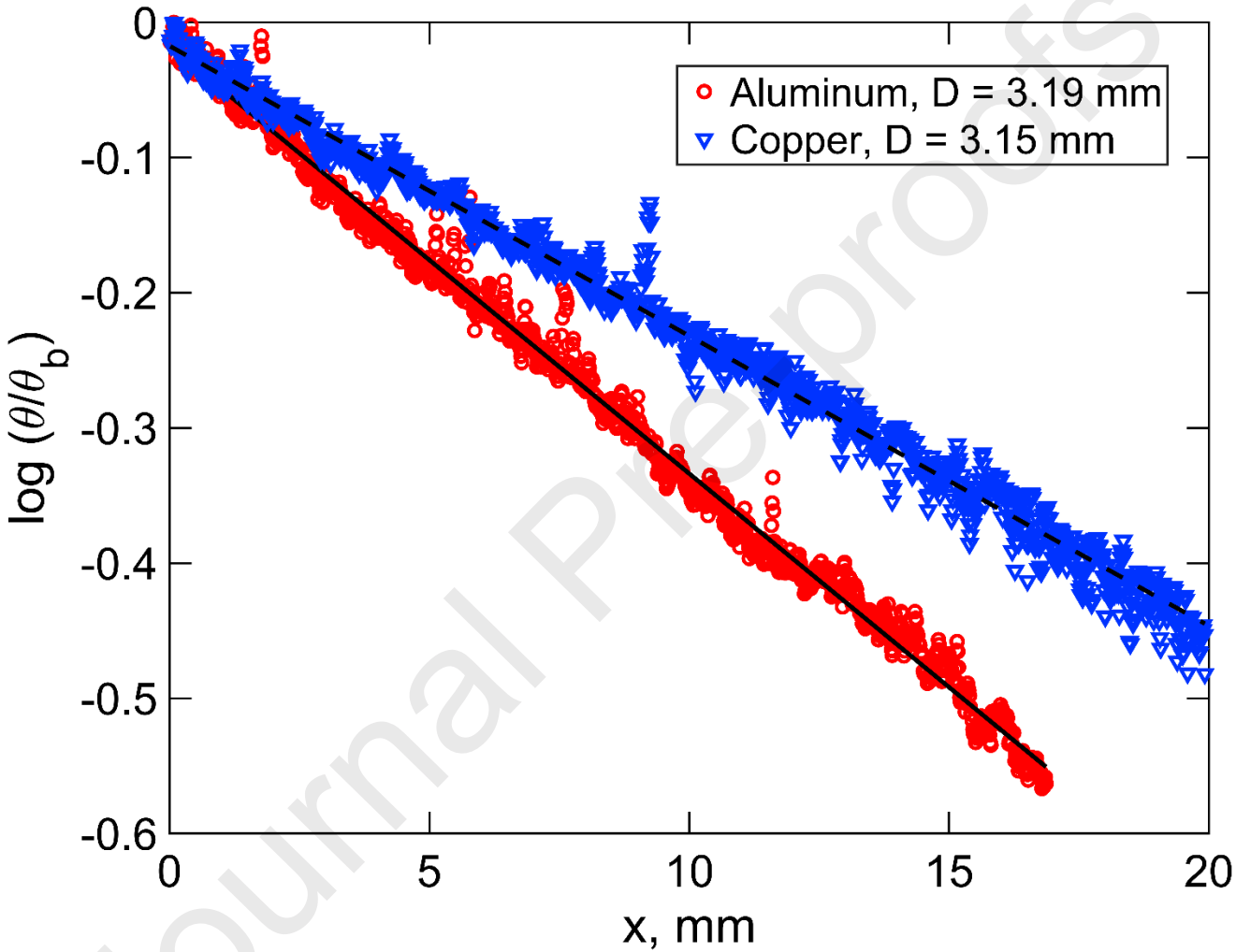

Figure 5: Measured temperature distributions in aluminum and copper wires of diameters 3.19 mm and 3.15 mm respectively. Data are plotted on a semilog scale, and linear curve fits are shown.

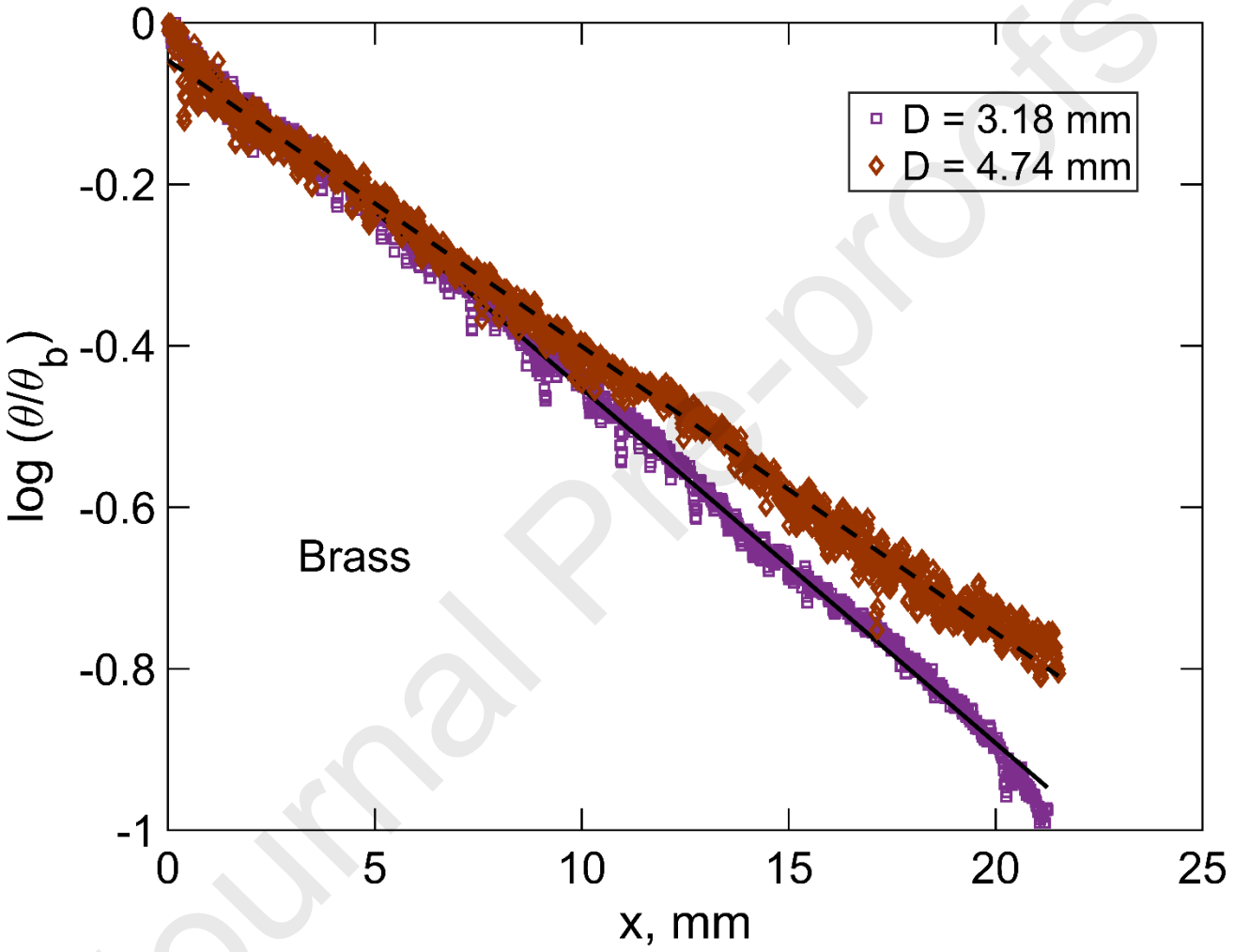

Figure 6: Comparison of temperature distributions of two Brass wires of significantly different diameters (3.18 mm and 4.74 mm), showing consistency with theoretical model.

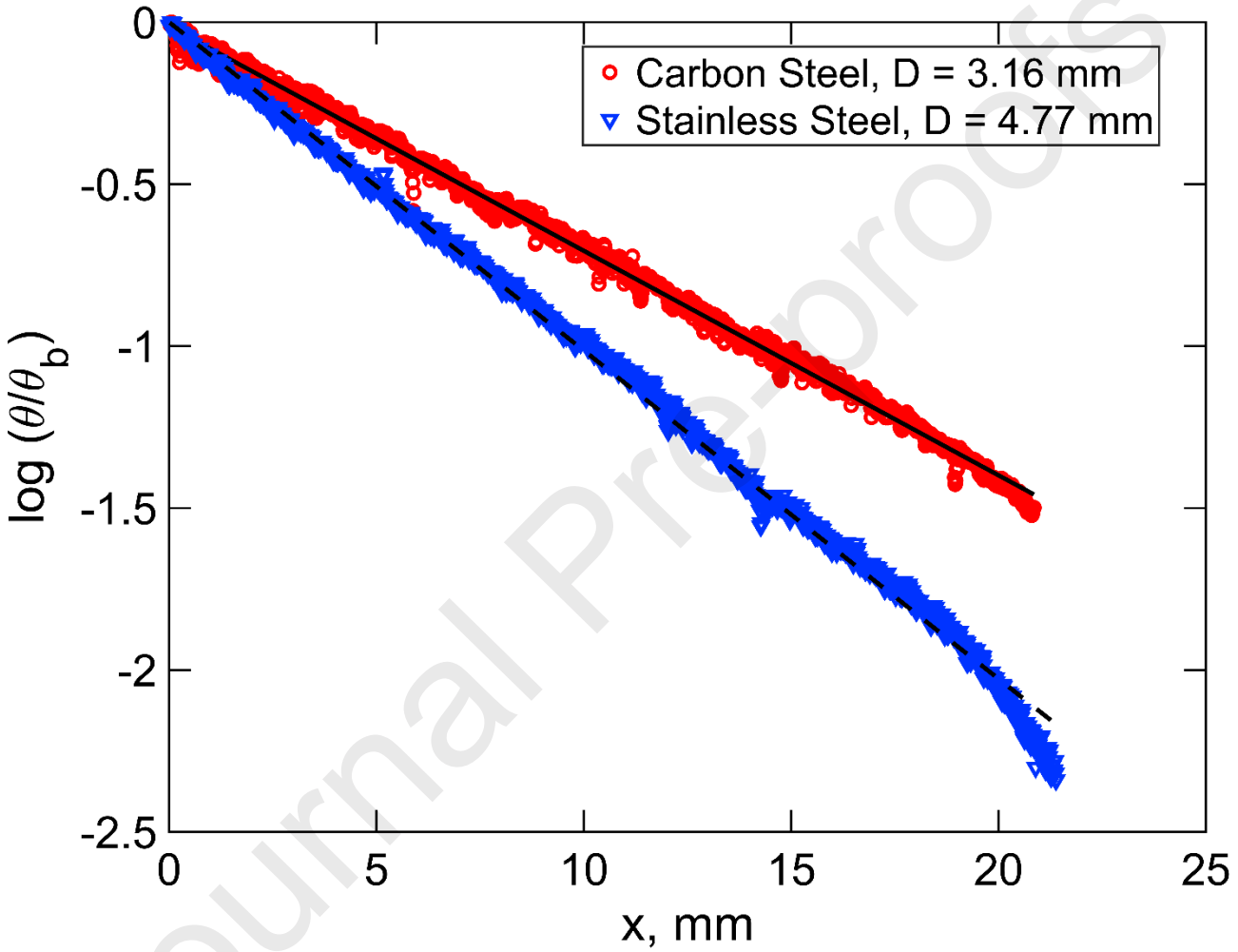

Figure 7: Comparison of temperature distributions of two wires of different materials and diameters (Carbon Steel, 3.16 mm and Stainless Steel, 4.77 mm)

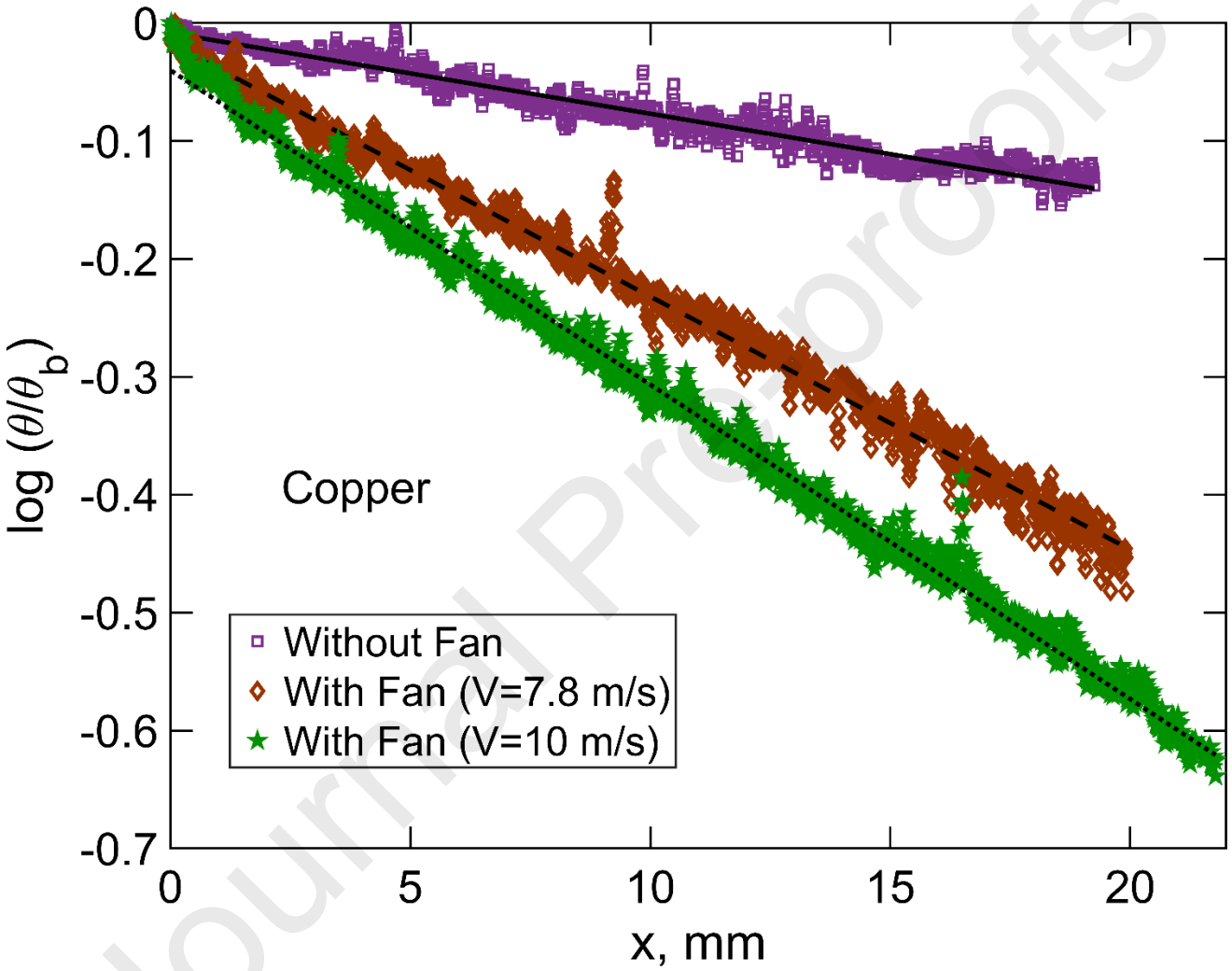

Figure 8: Measured temperature distributions for the same copper wire of 3.15 mm diameter in three different convective cooling conditions.

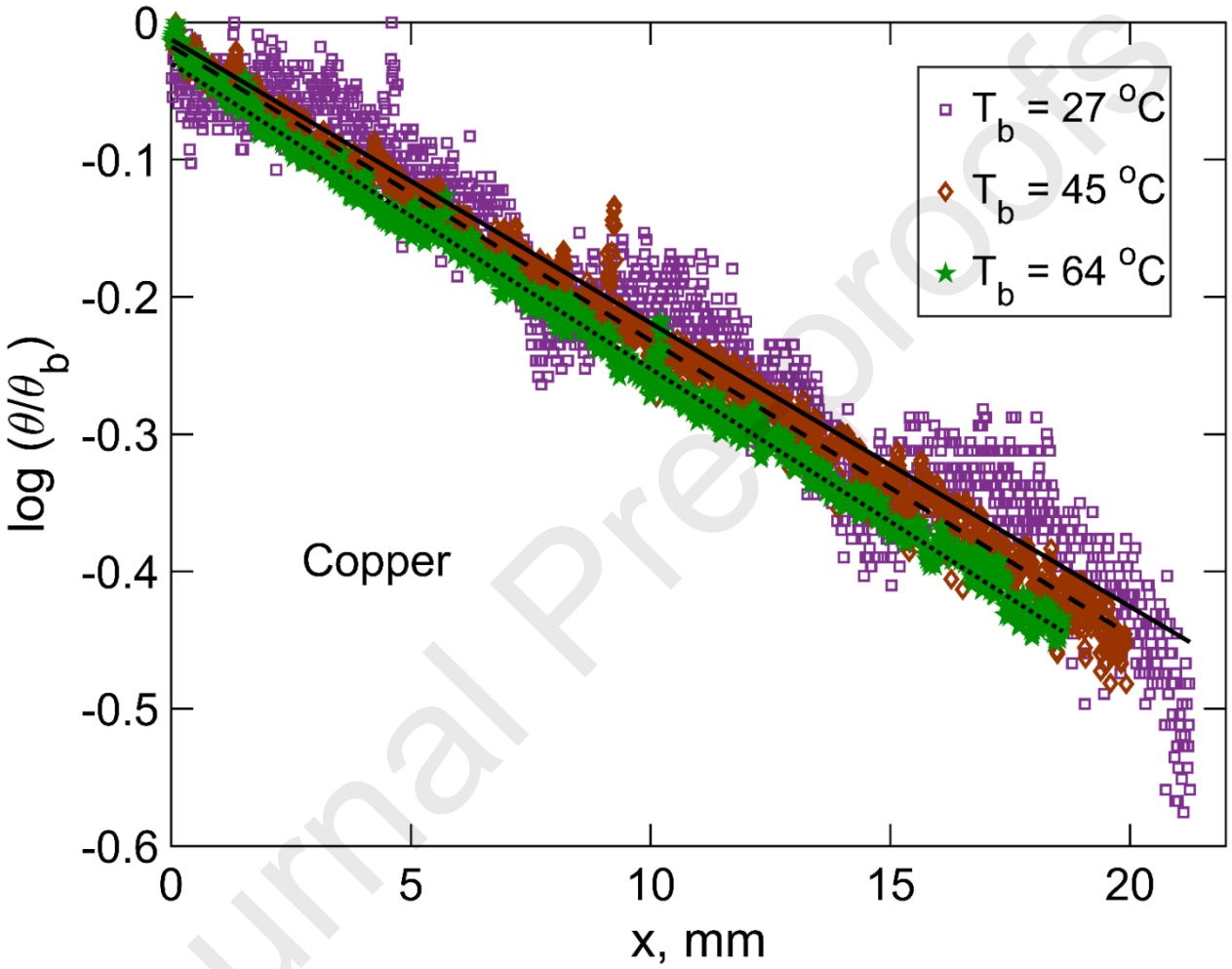

Figure 9: Measured temperature distribution for the same copper wire of 3.15 mm diameter with three different base temperatures. This plot shows the impact of base temperature on noise in the measured data.

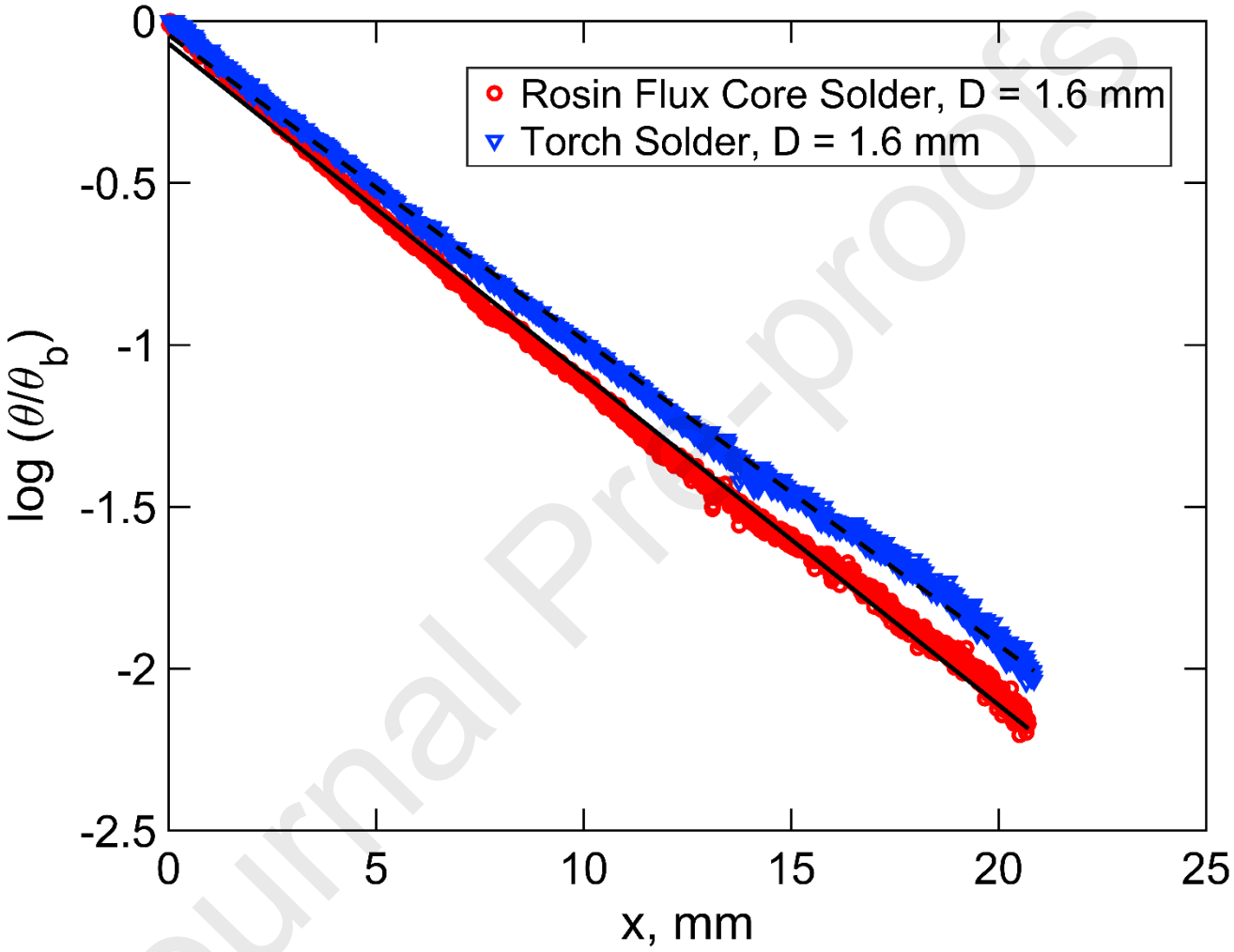

Figure 10: Measured temperature distributions in rosin flux core solder and torch solder wires of diameters 1.6 mm each. Data are plotted on a semilog scale, and linear curve fits are shown.

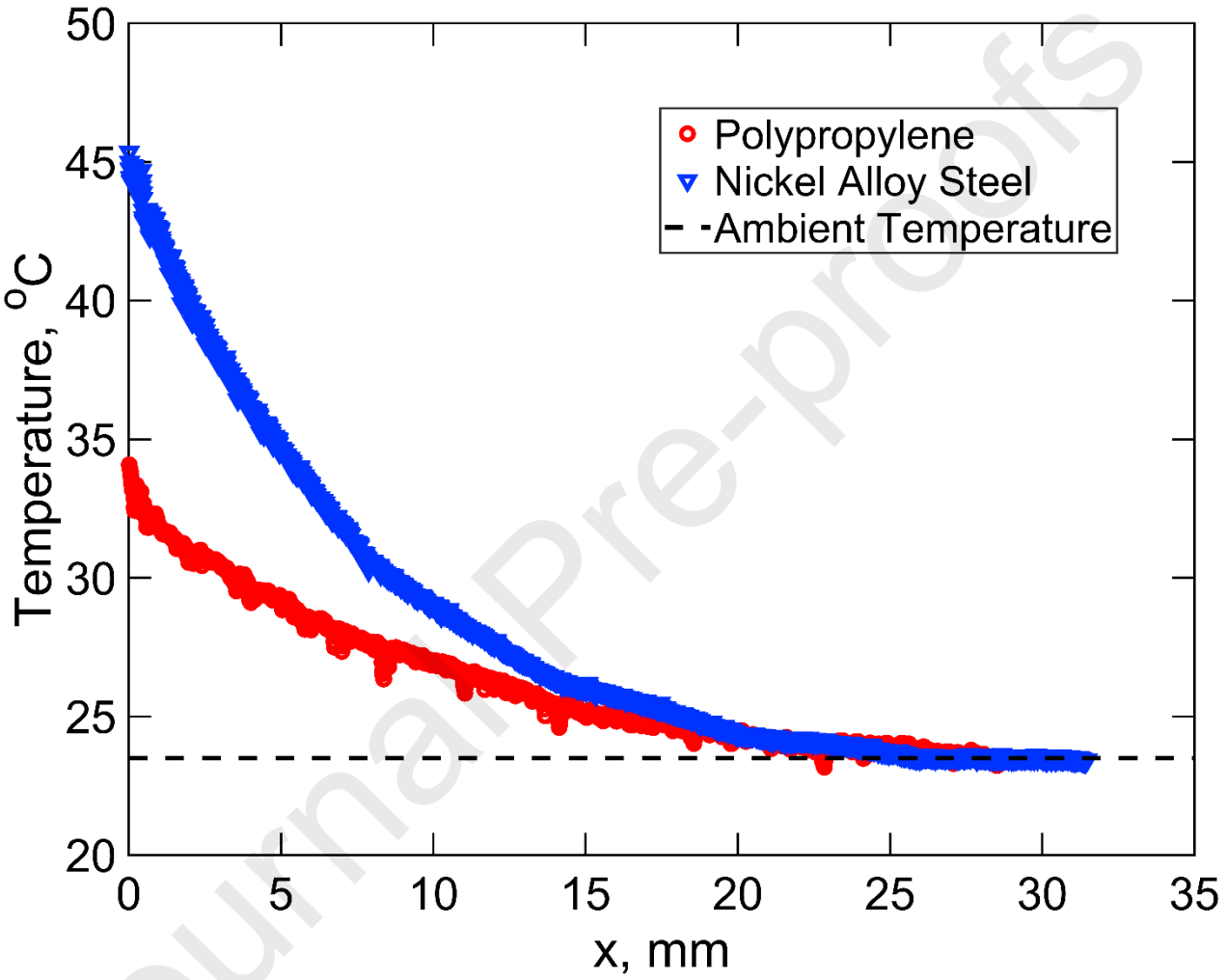

Figure 11: Temperature distributions in the entire length of polypropylene and nickel alloy steel wires for the validation of infinite fin assumption.

Table 1: Summary of measurements on a variety of metal wires using aluminum and carbon steel wires as standard.

Standard Wire			**Test Wire**				
Material	Diameter, mm	Thermal Conductivity, W/mK	Material	Diameter, mm	Thermal Conductivity, W/mK		
					Measurement	Manufacturer-provided value	% Deviation
Aluminum	3.19	182.7±9.1 (Laser Flash)	Copper	3.15	401.5±26.5	390.9	+2.7
			Carbon Steel	3.16	49.1±3.03	50.4	-2.7
			Brass	3.18	110.3±6.9	115.0	-4.1
Carbon Steel	3.16	45.8±2.3 (Laser Flash)	Alloy Steel	3.16	43.0±2.6	43.2	-0.5
			Stainless Steel	3.16	14.1±0.9	14.4	-2.5
			Nickel Alloy	3.18	11.0±0.7	10.1	+8.3

Table 2: Summary of measurements on a variety of polymer wires using polypropylene and PVC wires as standard.

Standard Wire			**Test Wire**				
Material	Diameter, mm	Thermal Conductivity, W/mK	Material	Diameter, mm	Thermal Conductivity, W/mK		
					Measurement	Independently measured value	% Deviation
Polypropylene	3.04	0.20±0.01 (Heat flux method)	Acetal	3.20	0.27±0.02	0.28	-3.6
PVC	3.05	0.14±0.01 (Heat flux method)	ABS	3.02	0.14±0.01	0.13	+3.3
			PTFE	3.24	0.16±0.01	0.17	-2.6

Table 3: Summary of measurements on a variety of solder wires using Carbon Steel wire as reference, for which a thermal conductivity of 45.8 W/mK is independently-measured using LFA technique.

Material	Composition	Diameter, mm	Measured Thermal Conductivity, W/mK
Machine Solder	Lead (70%), Tin (30%)	3.26	41.3±2.5
Solder for Drinking Water	Lead (0%), Tin (95%), Copper (4.8%), Silver (0.2%)	2.96	42.4±2.5
Rosin Flux Core Solder	Lead (60%), Tin (40%)	1.6	31.3±2.0
Torch Solder (without Flux)	Lead (60%), Tin (40%)	1.6	40.6±2.6

Highlights:

- Presents a method to measure thermal conductivity of a thin wire.
- Method utilizes infrared thermography and fin effect.
- Compares thermal response of test wire with a standard wire to determine thermal conductivity.
- Demonstrates capability of measurement for low and high thermal conductivity wires.
- Addresses an important metrology need for multiple engineering applications.